Article

Hydrodynamic and Sediment Modelling within a Macro Tidal Estuary: Port Curtis Estuary, Australia

Ryan J. K. Dunn *, Sasha Zigic, Murray Burling and Hsin-Hui Lin

RPS APASA Pty Ltd, P.O. Box 1679 Surfers Paradise, Queensland 4217, Australia;
E-Mails: szigic@apasa.com.au (S.Z.); mburling@apasa.com.au (M.B.); wlin@apasa.com.au (H.-H.L.)

* Author to whom correspondence should be addressed; E-Mail: rdunn@apasa.com.au;
Tel.: +61-(0)7-55-741-112.

Academic Editor: Billy Edge

Abstract: An understanding of sediment transport processes and resultant concentration dynamics in estuaries is of great importance to engineering design awareness and the management of these environments. Predictive modelling approaches provide an opportunity to investigate and address potential system responses to nominated events, changes, or conditions of interest, often on high temporal and spatial resolution scales. In this study, a three-dimensional hydrodynamic model and wave model were validated and applied to generate forcing conditions for input into a sediment transport model for the period 7 May 2010–30 October 2010 within a macro tidal estuary, Port Curtis estuary (Australia). The hydrodynamic model was verified against surface and near-bottom current measurements. The model accurately reproduced the variations of surface and near-bottom currents at both a mid-estuary and upper-estuary location. Sediment transport model predictions were performed under varying meteorological conditions and tidal forcing over a 180-day period and were validated against turbidity data collected at six stations within Port Curtis estuary. The sediment transport model was able to predict both the magnitudes of the turbidity levels and the modulation induced by the neap and spring tides and wind-wave variations. The model-predicted (converted) turbidity levels compared favourably with the measured surface water turbidity levels at all six stations. The study results have useful practical application for Port Curtis estuary, including providing predictive capabilities to support the selection of locations for monitoring/compliance sites.

1. Introduction

Estuarine environments are of great importance providing habitats (and nurseries) for numerous flora and fauna, including commercial and recreational fish species [1–3]. Estuaries also play a significant role in altering the flow of contaminants and sediments between terrestrial and coastal waters [4], moderating water quality [5], absorbing wave energy [6], providing relief from tidal surges [7,8], and providing cultural and recreational benefits [6]. Furthermore, the sheltered nature of estuaries often provides suitable settings for port and harbour infrastructure, which offer significant economic benefits in many parts of the world. However, the associated operations and expansions of large commercial ports and harbours often results in multiple environmental stresses, such as dredging to maintain navigable passage for larger ships, land reclamation, and changes in surrounding land use patterns altering sediment and nutrient runoff regimes [9–11].

An understanding of estuarine hydrodynamics and sediment transport dynamics is important since they play a critical role in the functionality and health of these systems. Knowledge of suspended sediment dynamics, influenced by tidal- and wind-driven currents and wave action [12–14], is essential for quantifying fluxes of substances and determining the fate of pollutants [15]. Re-suspension of bottom sediments have been demonstrated to influence productivity in shallow-water environments [16–18] through water column enrichment by nutrients originating from the sediment [19] and impacting light availability [20,21]. Additionally, re-suspension events potentially impact water quality through release of trace metals and organic contaminants [18,22], whilst also directly impacting on water column biota [23,24]. The re-suspension and transport of sediments can cause increased sedimentation, which is often mitigated by expensive dredging operations. In addition to navigational issues sediment re-susepsnion and sedimentation events may also lead to the mortality of benthic communities through smothering and burial [25].

As such, an understanding of transport processes and concentration dynamics in estuaries is of great importance to engineering design awareness and the management of these environments [22,26–28]. Mechanisms controlling the re-suspension, and deposition of fine sediments within tide-dominated estuaries are complex [28,29]. To date, considerable efforts have been invested to better understand the re-suspension mechanisms and transportation processes of sediments in estuarine settings (e.g., Ali *et al.* [29], Brand *et al.* [30], Giardino *et al.* [31], Guan *et al.* [32] and Hayter and Mehta [33]). The use and application of numerical models able to describe these physical processes (e.g., Carniello *et al.* [34], Cancino and Neves [35], Lumborg [36] and Le Normant [37]) are useful tools in planning and designing effective restoration and management strategies [38]. Specifically, predictive models provide an opportunity to investigate and address potential system responses (e.g., suspended sediment concentrations and bed level changes) to nominated events, changes, or conditions of interest, often on high-resolution temporal and spatial scales.

Located between Keppel Bay and Rodds Bay, Port Curtis estuary is an area of significant importance adjacent the World heritage listed Great Barrier Reef Marine Park along the central Queensland

coastline, Australia. In addition to being Australia's fifth largest multi-commodity port and the world's fifth largest coal export port in the world [39], the estuary is ecologically important for commercial and recreational fish species [40–42]. Furthermore, the estuary also supports visiting and local populations of vulnerable dugong (*Dugong dugon*) and endangered green turtle (*Chelonia mydas*) [43]. Activities surrounding Port Curtis estuary, including extensive mangrove and salt marsh reclamation for port infrastructure, marina, industrial and urban development, have altered the catchment, surrounding land use, and the estuarine conditions. According to the environmental and economic regional importance of the estuary and surrounding zones, the region has been the focus of recent scientific efforts [41–47]. Previously, Herzfeld *et al.* [47] provided an overview of the circulation characteristics and distributions of dissolved material using a pilot stage three-dimensional hydrodynamic model of the Port Curtis estuary. However, the modelling required further calibration and validation in order to achieve full confidence in solutions. To date a predictive understanding of ambient sediment dynamics within the system is still lacking.

In this paper, we first present a three-dimensional hydrodynamic model, Delft3D-FLOW and a wave model, SWAN, followed by a description of a versatile tailored sediment transport model, DREDGEMAP, used as part of this study. We then present the application of the model for describing the suspended sediment dynamics for the case study region of Port Curtis estuary. Thereafter, we compare the sediment transport model predictions under varying meteorological conditions and tidal forcing over a 180-day period to turbidity data collected at six stations within Port Curtis estuary. This is followed by estuary-wide snapshots of total suspended sediment concentrations during example spring and neap flood tide events.

2. Study Site

Port Curtis estuary is a macro tidal estuary (Figure 1) with energetic physical forcing, including; spatially- and temporally-variable waves, tidal currents, winds, and freshwater inputs. The estuary covers an area of approximately 200 km^2 and includes a network of rivers, creeks, inlets, shoals, channels, and islands. Depths range from <1 m on the intertidal flats to >20 m within the central channel, and a mean depth of 5.3 m. Tides are semi-diurnal, with a maximum tidal range of 4.69 m at Gladstone and up to 6.00 m within the Narrows [41]. The tide propagates into the estuary through the straits separating Facing Island from the mainland (Gatcombe Channel) and Curtis Island (North Channel), and through the Narrows via Keppel Bay in the north (Figure 1). Tides undergo a spring-neap cycle with a period of approximately 14 days, with maximum ranges during spring tides and ~1 m during neap tides. The strongest tidal currents are focused in the main tidal channels. Though a less frequent physical forcing mechanism compared to tidal forcing, which causes most of the estuarine mixing, freshwater inputs are occasionally important during periods of high rainfall (*i.e.*, summer months). Freshwater flows originate from the Narrows as a result of the nearby Fitzroy River flooding, the Calliope River and Auckland Creek which discharges into the estuary through Gladstone (Figure 1). The large tides ensure that the water column is vertically well mixed, and are also responsible for significant re-suspension of fine sediment [47]. Combined with very large deposits of silt from the hinterland in times of flood, the estuary maintains a highly turbid character. The estuary is characterised by extensive areas of tidal flats that become exposed at low tide and large areas of mangroves fringing the estuary, which behave as a

storage buffer for water at high tide. Port Curtis estuary sediments consists primarily of silts and clays within the shallow intertidal banks, while fine and course sand predominant the more tidally energetic deeper regions of the estuary. Additionally, the estuary is influenced by local wind-driven waves, which contribute to turbulences and sediment suspension events. Wave activity is greatest during periods of prolonged south-easterly trade winds.
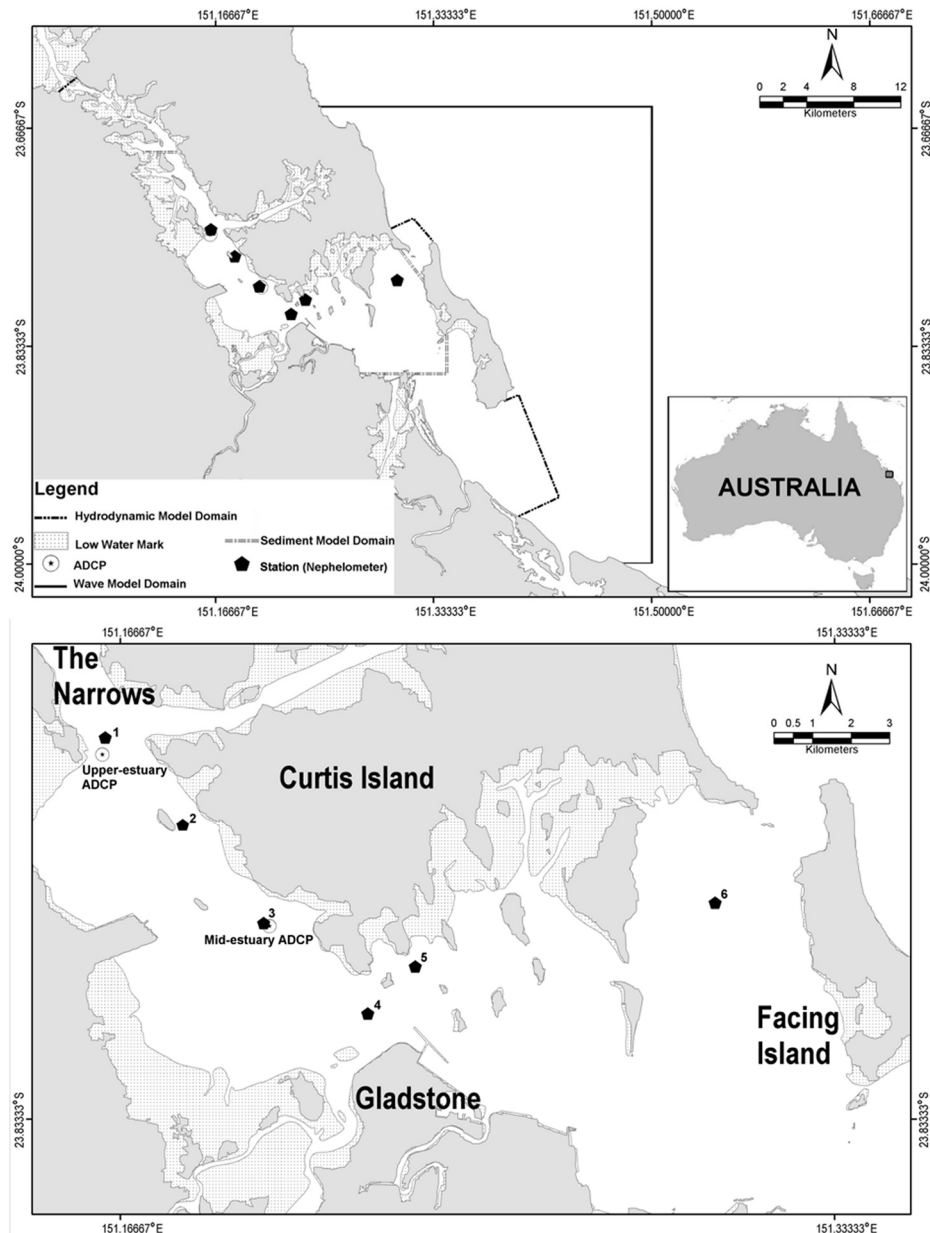

Figure 1. Site study map showing location of Port Curtis estuary indicating the model domain extents, ADCP site locations and surface waters turbidity measurement stations.

3. Model Description

A hydrodynamic model and wave model in conjunction with a sediment transport model were used during this study. Firstly, a hydrodynamic and wave model was used to simulate complex current flows and wave actions throughout the estuary subject to tidal flows and prevailing metocean conditions within Port Curtis estuary. Thereafter a versatile tailored sediment transport model, DREDGEMAP [48], was

coupled with the hydrodynamic and wave models over a 180-day duration to model suspended sediments throughout Port Curtis estuary.

3.1. Hydrodynamic Model

The hydrodynamic conditions were simulated using Delft3D-FLOW [49]. The model has been successfully applied within oceanic, coastal, estuarine, riverine, and flooding conditions [49–51]. A curvilinear computational grid with varying cell size was developed for the entire extent of the estuary. The finest grid resolution (25 m) was defined along shorelines and regions of steep depth gradients, to accurately define the current patterns. Whilst the coarsest resolution (~400 m) was applied in the outer region nearby the southern entrances of the estuary and neighbouring coastal waters (Figure 1). Datasets used to represent the bathymetry of the estuary were sourced from commercial nautical charts and bathymetric surveys [52]. In order to define the three-dimensional current structure, a σ-layer approach was employed with five equally-proportioned vertical layers throughout the model domain. Tidal variations were driven at the open boundaries of the model domain through the northern entrance using water elevation data from Port Alma tidal station (23.58° S, 150.87° E) and the eastern entrances using data from the Gatcombe Head tidal station (23.88° S, 151.37° E).

The "cyclic" advection schemes for momentum and transport were selected. The κ-ε turbulence closure scheme was selected for the vertical viscosity formulation, with background values set to 0 m^2/s. The Manning roughness formula was used to account for the bottom friction, with a uniform coefficient of 0.02 selected as representative of the seabed in the region on the basis of previous works by Wolanski *et al.* [53] and King and Wolanski [54]. The horizontal eddy viscosity was set to 1 m^2/s throughout the model domain. Hourly wind speed and direction data, measured at the Gladstone Airport by the Australian Bureau of Meteorology (station identification: 039326; 23.87° S, 151.22° E), was used to account for the wind forcing across the model domain. The wind drag coefficients, C_D, is assumed to vary linearly with wind speed from 0.00063 to 0.00723 over the range of U_{10} = 0–100 m/s. The model time-step was set to 0.2 min, which produced Courant numbers less than 10.

3.2. Wave Model

The SWAN model [55] was used to reproduce the prevailing wave conditions. The model is fully spectral (in all directions and frequencies) and computes the evolution of wind waves in coastal regions with shallow water depths. The physical processes selected for the simulations were: white-capping, depth-induced wave-breaking, bottom friction, and triad wave-wave interactions. Using an unstructured triangular mesh approach, the generated computational grid included the entire Port Curtis estuary and offshore regions (24.00° S, 151.50 °E to 23.65° S, 151.50° E, Figure 1). A fine (<50 m) mesh resolution was defined for tidal creeks and shorelines and a coarser mesh resolution (>500 m) was applied over the estuary region and near the open boundaries of the domain. The bathymetric dataset used for the wave model was sourced, as per the hydrodynamic modelling. Surface waves entering the model boundaries were obtained from the WAVEWATCH III® (WW3) global model (National Centres for Environmental Prediction National Oceanic and Atmospheric Administration, College Park, MD, USA) [56]. Outputs of WW3 (significant wave height (H_s), mean wave period (T_p) and peak wave direction period (P_{dir})) were extracted from the computational point closest to the area of interest (24.00° S, 152.50° E) and

used for the model simulations. Model surface and open boundary data were updated at hourly intervals. The default SWAN parameterisation of depth-induced wave-breaking was employed (0.73 [57]). Bottom friction was activated using the drag law-based model of Collins [58] and a bottom friction coefficient of 0.01 was applied. In addition, quadruplet wave-wave interaction was also included. Hourly wind speed and direction data, measured at the Gladstone Airport by the Australian Bureau of Meteorology, was used as model input.

3.3. Sediment Transport Model

Suspended sediment concentrations (SSC) were modelled using a tailored version of DREDGEMAP, an enhancement of SSFATE [48], a three-dimensional sediment transport and fates model, jointly developed by Applied Science Associates Pty Ltd and the U.S. Army Corps of Engineers (USACE) Environmental Research and Development Center (ERDC). The model has been successfully applied in coastal and estuarine settings [59–61]. The model represents the total mass of sediments suspended over time by a defined sub-sample of Lagrangian particles, allocating an equal proportion of the mass to each particle, where the transport, dispersion and settling of suspended sediment released to the water column is calculated using a random-walk procedure. Sediment particles are divided into five size classes. For the purpose of this study the following grain size classes were adopted: 5 μm, 75 μm, 200 μm, 450 μm and 1000 μm.

Settling of mixtures of particles is a complex process due to interaction of the different size classes, some of which tend to be cohesive, and thus clump together to form larger particles that have different fall rates than would be expected from their individual sizes. Enhanced settlement rates, due to flocculation and scavenging, are particularly important for clay and fine-silt sized particles and as such these processes are implemented in DREDGEMAP.

Minimum sinking rates are calculated using Stokes equations, based on the size and density of the particle. However, sinking rates of finer classes (representing clay and silt-sized particles) are increased based on the local concentration of the same and larger particles, to account for clumping and entrainment.

The settling velocity of each particle size class (Ws_i), is computed from:

$$Ws_i = a\left(\frac{C}{\bar{C}}\right)^{n_i} \tag{1}$$

$$a = \frac{1}{C}\sum_i a_i C_i \tag{2}$$

$$\bar{C}_{ul} = \frac{1}{C}\sum_i C_{uli} C_i \tag{3}$$

$$\bar{C}_{ul} = \frac{1}{C}\sum_i C_{lli} C_i \tag{4}$$

where: C_{uli} and C_{lli} are the nominal upper and lower concentration limits, respectively, for enhanced settling of grain size i, a_i is a grain-size class average maximum floc settling velocity, C is the total concentration for all grain size classes [61].

$$Ws_i = a \tag{5}$$

whereas, if $C \leq \bar{C}_{ul}$ then

$$Ws_i = a \left(\frac{\bar{C}_{ll}}{\bar{C}_{ul}} \right)^{n_i} \tag{6}$$

Selected values for C_{uli}, C_{lli} and a_i adopted for this study ranged between 1000–8000 mg/L, 50–400 mg/L and 0.0008–0.1 m/s, respectively. The settling velocity for the largest size class (1000 μm) was assumed constant at 0.1 m/s.

Deposition is calculated as a probability function of the prevailing bottom stress, local sediment concentration and size class. Mixing of re-suspended sediment into the water column is a dynamic balance between estimates of the sinking rate and vertical mixing induced by turbulence (as specified by vertical mixing coefficients).

Sediment deposition flux is computed as:

If $0 \leq P_i \leq 0.05$, then

$$Flux_i = \frac{C_i Flux_{i+1}}{C_{i+1} + 1} \tag{7}$$

Otherwise,

$$Flux_i = b_i C_i Ws_i P_i \tag{8}$$

where: P_i is the deposition probability of *i*-th size class, C_i is the sediment concentration, Ws_i is the calculated settling velocity and b_i is the empirical parameter that includes all other factors influencing deposition other than shear (0.2–1.0 for clays to fine sand) [61].

Deposition probability, P_i, is calculated as follows:

P_1, for clay sized particles (1st size class)

$$P_1 = \left(1 - \frac{\tau}{\tau_{cd}}\right), \text{if } \tau < \tau_{cd} \tag{9}$$

$$P_1 = 0, \text{if } \tau > \tau_{cd} \tag{10}$$

where: τ_{cd} is the critical shear stress for deposition for the clay fraction, for this study a value of 0.016 was adopted. The bottom shear stress is based on the combined velocity due to current and wave action using the parametric approximation by Soulsby [62].

P_i, for the other size classes (2nd, 3rd and 4th size classes)

$$P_i = 0, \text{if } \tau \geq \tau_{uli} \tag{11}$$

$$P_i = 1, \text{if } \tau \leq \tau_{lli} \tag{12}$$

where: τ_{uli} is the shear stress above which no deposition occurs for grain size class *i*, and τ_{lli} is the shear stress below which deposition probability for grain class *i* is 1.0.

For values between τ_{lli} and τ_{uli}, linear interpolation was used. Adopted τ_{uli} and τ_{lli} values for this study ranged between 0.030–0.900 and 0.016–0.200, respectively, excluding the 1000 μm size class.

The model can employ two different re-suspension algorithms. The first is based on the work of Sanford and Maa [63] and, subsequently, Lin *et al.* [64], and applies to material deposited in the last tidal cycle, which accounts for the fact that newly deposited material will not have had time to consolidate and will be re-suspended with less effort (lower shear force) than consolidated bottom

material. The second algorithm, which was used in this study, is the established Van Rijn method [65] and applies to all other material that has been deposited prior to the start of the last tidal cycle. This method calculates a constantly varying critical threshold for re-suspension, based on the median local particle-size distribution for settled material. Re-suspension algorithms implemented in DREDGEMAP are presented in detail by Swanson *et al.* [61].

Knowledge of the initial bed sediment distribution was critical in predicting suspended sediment concentrations. Surface sediment grain size contribution maps were established based on data sourced from the analysis of >650 sediment cores collected throughout the estuary [66]. The contribution of five sediment size classes (5 μm, 75 μm, 200 μm, 450 μm and 1000 μm) throughout the estuary was spatially assigned and interpolated using the inverse distance weighting method [67] throughout the model domain. A grid resolution of 40 m was used throughout the model domain. Clays and silts dominate the shallow intertidal regions of the estuary, whilst larger sediments, including fine and coarse sands dominate the more energetic deeper channel regions of the estuary. Figure 2 presents the median grain size (D_{50}) of the surface sediments of Port Curtis estuary used as part of the study. Measured sediment densities were incorporated into the model inputs. The sheltering effects of seagrass on shear stress [68] and biologically-altered erodability of the bed sediments [69,70] was not included as part of the modelling approach.
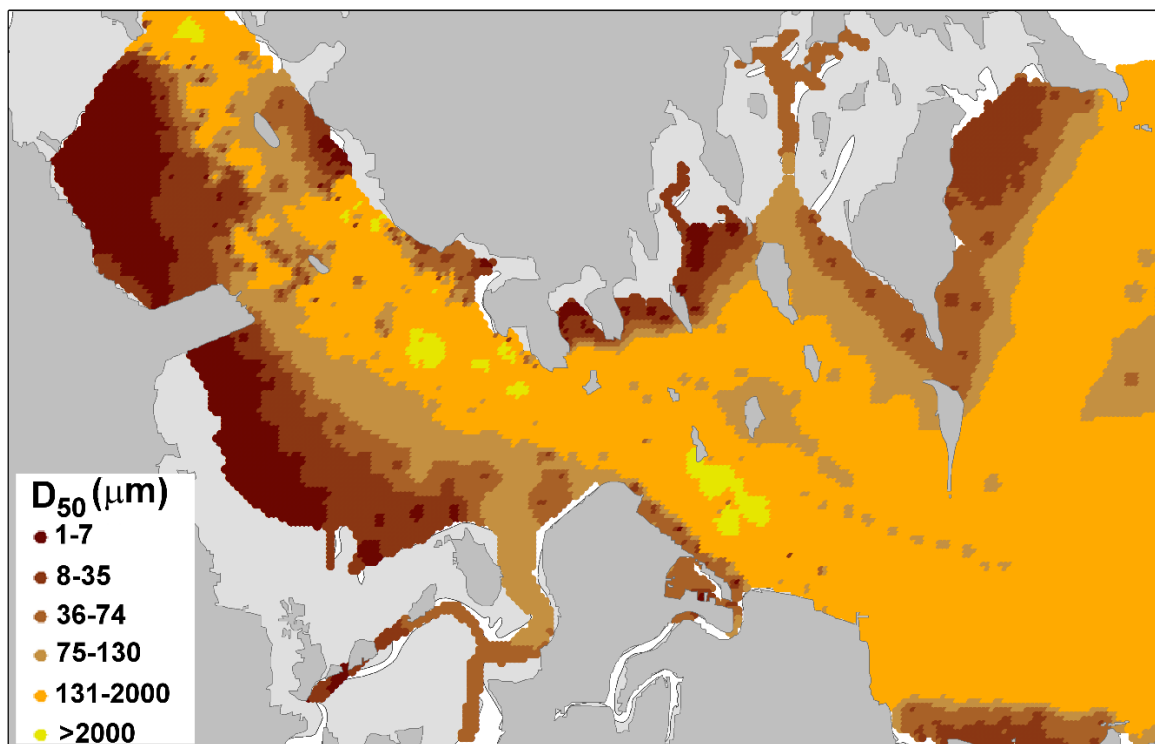

Figure 2. Surface sediment median grain size (D_{50}) map of Port Curtis estuary (October 2010).

Model predictions output as SSC were converted to turbidity in order to provide comparison with coincident turbidity datasets collected at six stations. Suspended sediment concentrations were converted as follows [71]:

$$Predicted\ NTU = Predicted\ suspended\ sediment\ concentration\ \times 0.5477 \qquad (13)$$

4. Model Validation

Measured data was used to validate the models and to verify their ability to predict prevailing conditions.

4.1. Hydrodynamic Model

Model-predicted currents were verified using measured Acoustic Doppler Current Profiler (ADCP; seafloor mounted Teledyne RD ADCPs) data collected between 7th to 27th October 2010 at a mid-estuary (23.78833° S, 151.20142° E; depth ~7.5 m) and upper-estuary site (23.74817° S, 151.16243° E; ~10.0 m) (Figure 1). The model accurately represented the semi-diurnal mixed spring and neap tides throughout the 21-day deployment period, as well as variations of the surface and near-bottom current speeds and directions during the deployment period. Analysis of the measured data revealed greater current speeds in the upper layers of the water column in comparison to the lower depth layers at both sites with maximum surface current speeds exceeding 1 m/s and near-bottom speeds approaching maximum speeds of 0.8 m/s. Predominant flow directions were northwest and southeast, which corresponds to the orientation of the adjacent coastline, occurring during the flood and ebb tide, respectively. Directional differences were observed between depth layers during the time-series as a result of wind influences and bathymetry-induced steering.
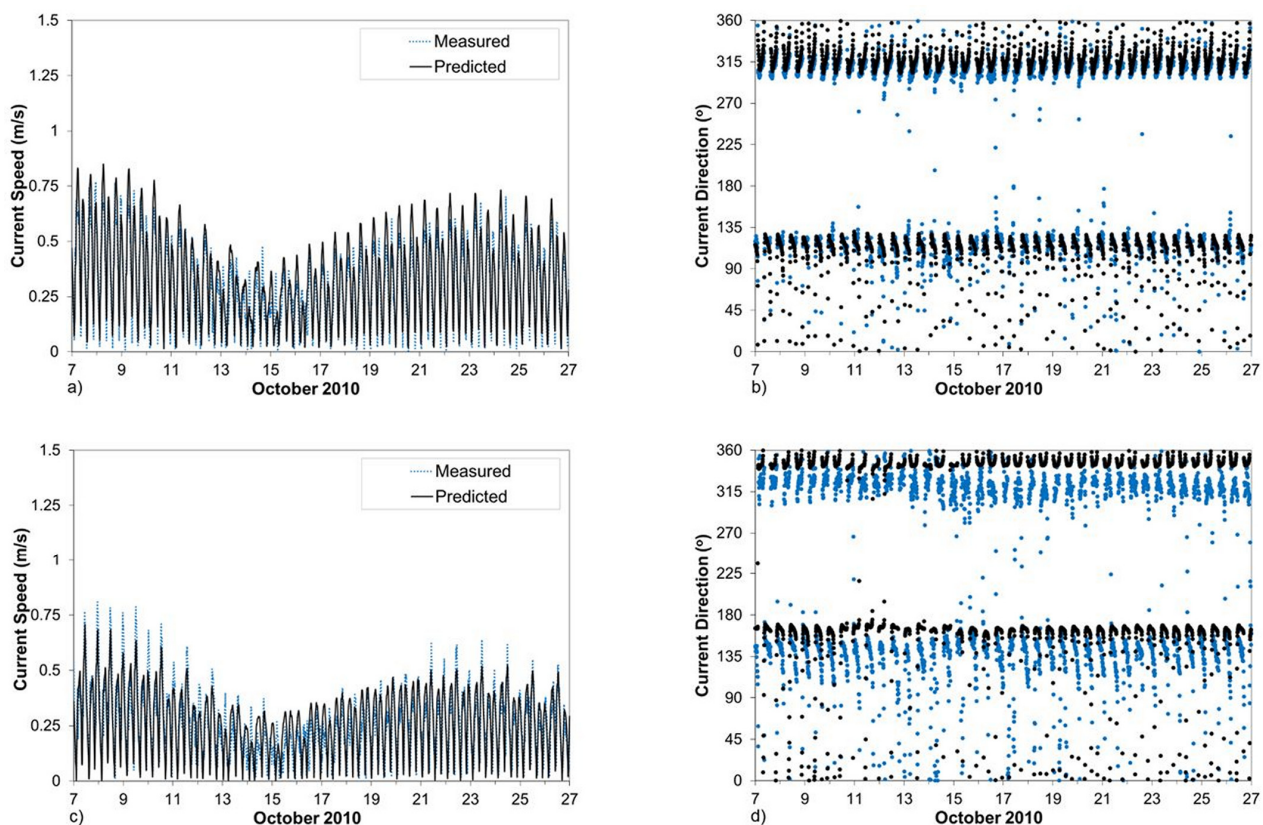

Figure 3. Comparison between measured and predicted near-bottom current speeds (**a**,**c**) and direction (**b**,**d**) at the mid-estuary and upper-estuary ADCP sites. The data is compiled from the measured and predicted datasets 07 October 2010–27 October 2010.

To provide a quantitative assessment of the performance of the hydrodynamic model, the correlation coefficient (R), Index of Agreement (IOA; Willmott [72]) and Mean Absolute Error (MAE; Willmott [73]) were calculated for surface and near-seabed currents.

Comparison between the measured and predicted surface elevation at both the mid-estuary and upper-estuary sites demonstrated very good agreements (Figure 3). Statistical analyses between the measured and predicted elevation datasets produced R, IOA, and MAE values of 0.99, 0.99, and 0.17 at the mid-estuary site and 0.99, 0.98, and 0.25 at the upper-estuary site, respectively. Additionally, the current speeds and direction were shown to be satisfactorily reproduced with IOA values for current speed ranging between 0.82–0.90 and direction ranging between 0.93–0.97 for both sites and depth layers compared. Table 1 provides a summary of the results of the statistical analysis performed. The performance of the model indicates the suitability for input into the sediment transport model.

Table 1. Hydrodynamic model performance summary. The data is compiled from the measured and predicted datasets 07 October 2010–27 October 2010.

Site	Depth Layer	Current Speed		
		R	IOA	MAE
Mid-estuary	Surface	0.81	0.90	0.12
	Near-seabed	0.92	0.92	0.07
Upper-estuary	Surface	0.69	0.82	0.12
	Near-seabed	0.78	0.88	0.08
Site	Depth Layer	Current Direction		
		R	IOA	MAE
Mid-estuary	Surface	0.91	0.95	30.25
	Near-seabed	0.96	0.97	16.43
Upper-estuary	Surface	0.89	0.93	31.61
	Near-seabed	0.91	0.94	35.42

4.2. Wave Model

In the absence of inshore wave data, the model accuracy was verified using measured wave data between December 2009 to March 2010 offshore Port Curtis estuary (23.89562° S, 151.50238° E [74]). Table 2 provides a summary of the results of the statistical analysis performed using the measured and predicted wave parameters offshore Port Curtis estuary. The model was shown capable of replicating the general trend at the offshore wave buoy. Predicted long-period ocean waves ranged from ~1 to 4 m in height, with the predicted peak wave direction being ~90°. Due to the orientation of the estuary entrance, long-period ocean swells are typically blocked by Facing Island and the mainland coastline south of Port Curtis and, as such, ocean wave penetration is negligible. The wave climate within the estuary is, therefore, typically dominated by locally generated wind waves. The maximum fetch within the estuary (~20 km) is achieved by southeast winds, which are one of the predominant wind directions of the region [75]. Significant wave heights within the estuary have been documented as being <0.5 m and <0.3, ~96% and ~80% of the time, respectively, with wave periods less than 5 s [76]. The modelled estuary wave climate demonstrated H_s typically ranging between <0.01–0.5 m with an average H_s value

of ~0.2 m within the mid-estuary region. The mean wave period typically ranged between 1 and 4 s within the model domain.

Table 2. Wave model performance summary. The data is compiled from the measured and predicted datasets 01 October 2009–30 March 2010.

Parameter	R	IOA	MAE
Significant wave height (H_s)	0.82	0.59	0.80
Peak wave period (T_p)	0.54	0.72	1.40
Peak wave direction (P_{dir})	0.93	0.94	18.49

4.3. Sediment Transport Model

The sediment transport model was calibrated and compared against turbidity surface water (~0.5 m depth from surface) measurements collected at six different stations within Port Curtis estuary (see Figure 1 and Table 3). Stations were deployed and maintained as part of a Port Curtis estuary monitoring program using YSI 6920 sondes with 650MDS data loggers (YSI Australia, Brisbane) e.g., [77]. The modelling considers an extended period characterised by different tidal and meteorological conditions over a 180-day period. In order to illustrate and quantify the model's performance, the results of the simulations were compared to the measured data, based on both hourly-measured datasets (Figure 4) and based on an exponentially-weighted moving average (EWMA) (6 h) (Figure 5). The model-predicted turbidity levels compare favourably with the measured data. The model predicted both the magnitudes of the turbidity levels and the modulation induced by the neap and spring tides and wind-wave variations. As the six turbidity stations were well distributed within the estuary and positioned in locations with varying initial surface sediment grain size composition, water depth, bottom topography, and wind wave fetches, the comparison between the model-predicted and measured turbidity levels is considered a rigorous assessment.

Table 3. Station summary of measured turbidity dataset used as part of sediment transport model validation.

Station	Latitude (°S)	Longitude (°E)	Water Depth [HAT (m)]
1	23.74802	151.16267	7
2	23.76538	151.18108	7
3	23.78768	151.19993	5
4	23.80845	151.21712	6
5	23.79588	151.23862	8
6	23.78308	151.30653	6

Where HAT represents highest astronomical tide.

Model performance was assessed by determining R, IOA, and MAE values at each station based on the hourly measured and predicted turbidity datasets. Table 4 provides a summary of statistical analysis performed using the measured and predicted turbidity hourly datasets at the six stations within Port Curtis estuary. Statistical analyses between the measured and predicted hourly and EWMA datasets produced R values ranging between 0.07–66 and 0.17–0.75, IOA between 0.22–0.68 and 0.30–0.83, and

MAE ranging between 7.07–12.57 and 4.96–8.14, respectively. Generally the model performed best in the mid-estuary region.
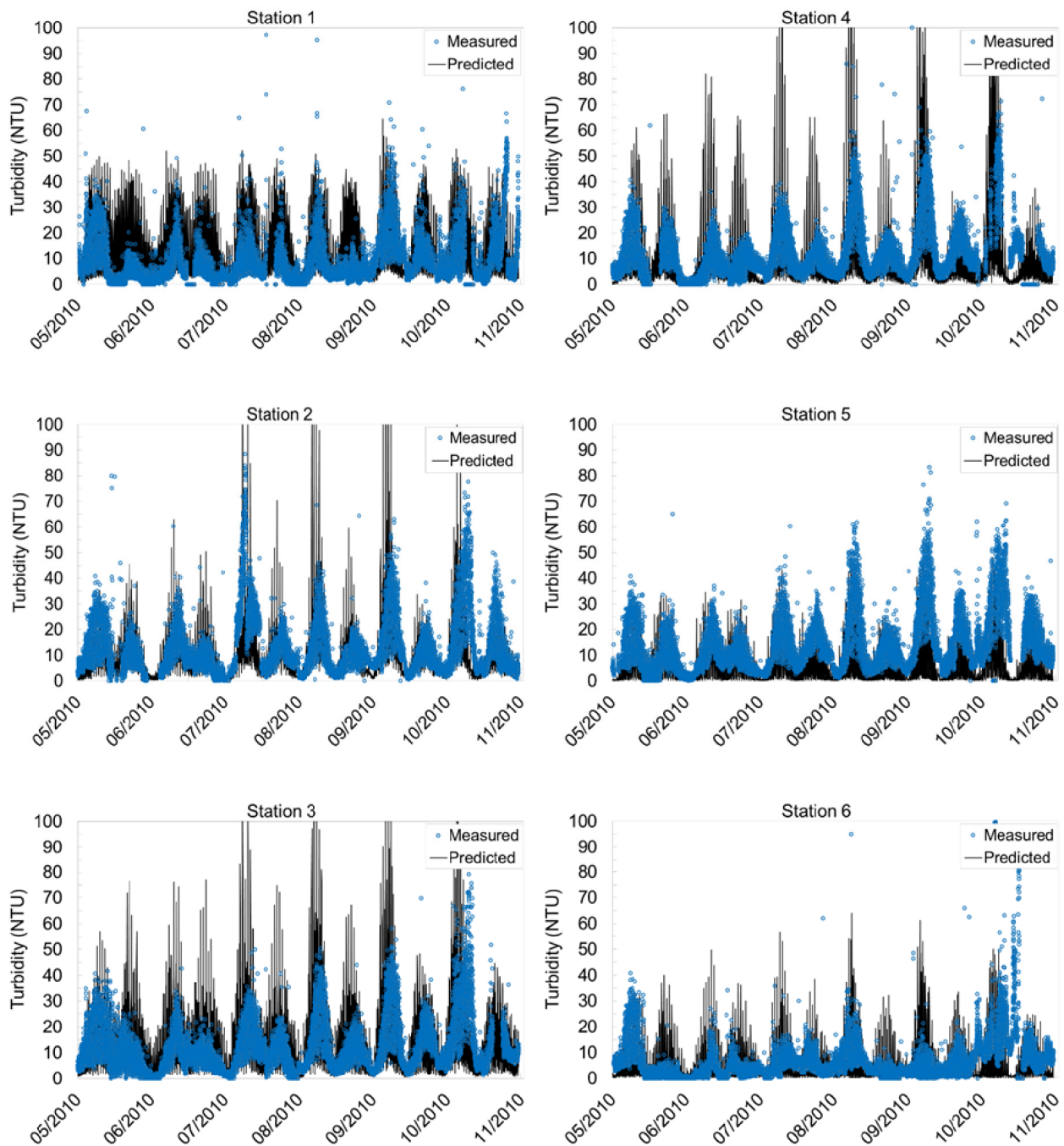

Figure 4. Comparison between the measured and predicted surface turbidity based on turbidity hourly datasets at the six stations (Stations 1–6). The data is compiled from the measured and predicted datasets 07 May 2010–30 October 2010.
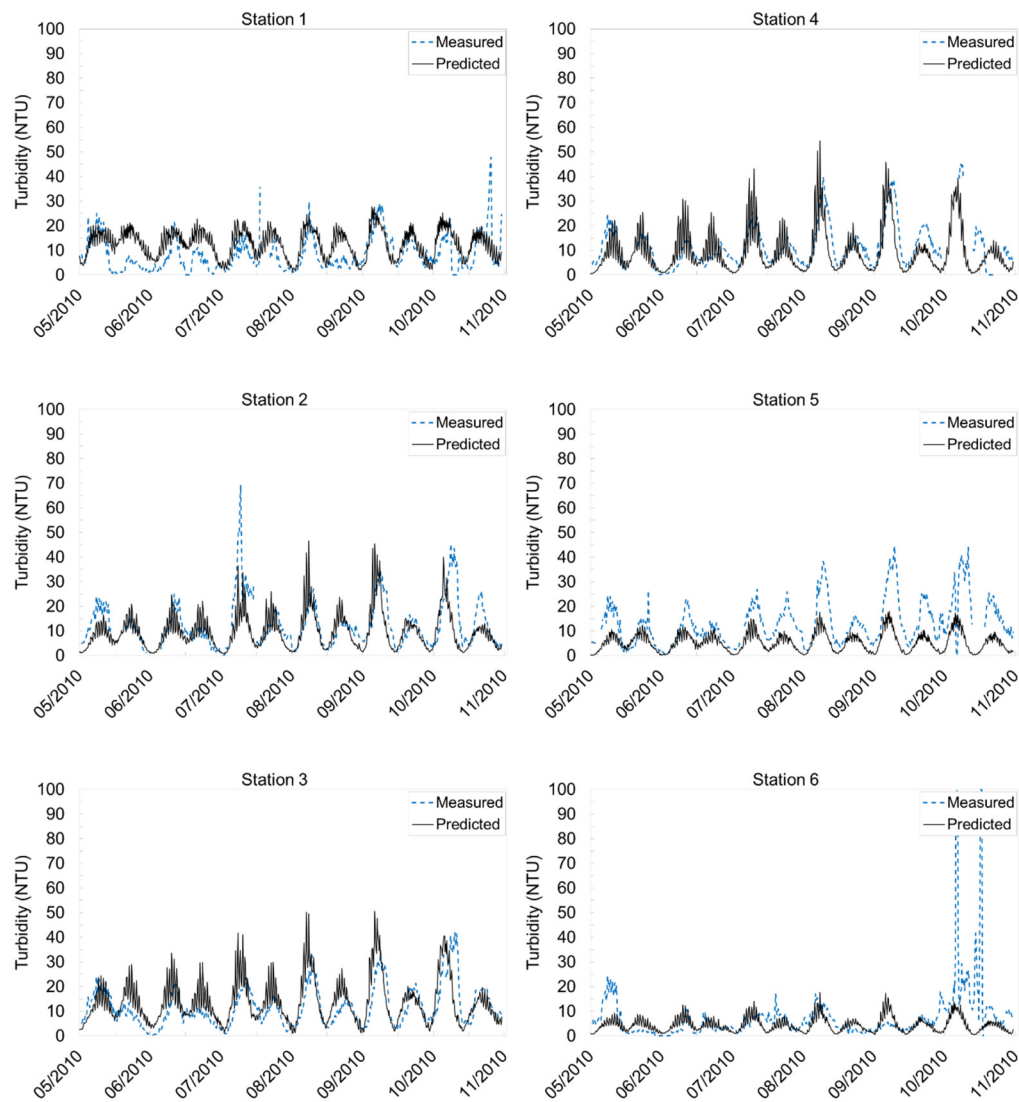
Figure 5. Comparison between the measured and predicted surface turbidity based on 6 h measured datasets. The data is compiled from exponentially-weighted moving average turbidity hourly datasets at six stations (Stations 1–6) from the measured and predicted datasets 07 May 2010–30 October 2010.

Once suspended from the estuary floor, the fate of the suspended sediments is dependent on factors, including particle size and associated settling velocity, ambient current speed and direction, and water depth. Larger particles typically located within the deeper more energetic regions settle more quickly once re-suspended, while the finer particles that are re-suspended remain suspended and are transported greater distances and settle during decreased current speeds and wave action.

Although the model-predicted turbidity levels compared favourably with the measured surface data, the model does possess limitations in terms of included turbidity sources. Areas identified that require further inclusion into the transport model include; sediment loadings from freshwater inflow, biological production of suspended particulate matter owing to algal growth, bioturbation, and inclusion of seagrass/biological influence on bed shear and re-suspension. Furthermore, dredging and ship traffic-induced sediment re-suspension, which may also affect suspended sediment dynamics, was not considered as

part of the model. Despite the exclusion of contributing turbidity sources associated with the model, the modelling illustrates the importance of the tidal-induced currents and wind-wave interactions on sediment re-suspension and the applicability of the model in predicting turbidity levels within Port Curtis estuary. Reduced discrepancies between the measured and predicted turbidity levels may be achieved following the model adoption of established site-specific relationships (conversions) between measured SSC and turbidity levels. Such an understanding would prove very important for the model's performance when reporting turbidity levels and also provides flexibility in the model's application.

Table 4. Sediment transport model performance summary based on the comparison between measured and predicted hourly turbidity datasets and exponentially weighted moving average (6 h). The data is compiled from the measured and predicted datasets 07 May 2010–30 October 2010. Location of measurement stations are shown in Figure 1.

Station	Hourly Datasets		
	R	IOA	MAE
1	0.07	0.22	7.07
2	0.51	0.68	8.97
3	0.66	0.57	12.57
4	0.47	0.58	12.28
5	0.50	0.50	10.02
6	0.13	0.25	7.17
Station	Exponentially Weighted Moving Average (6 h)		
	R	IOA	MAE
1	0.49	0.64	6.19
2	0.63	0.75	5.19
3	0.71	0.83	4.98
4	0.75	0.80	5.33
5	0.74	0.58	8.14
6	0.17	0.30	4.96

5. Results and Model Applications

5.1. Hydrodynamic Conditions

The verified hydrodynamic model (and wave model) was used to generate current data as inputs into the sediment transport model. The modelled period was selected to coincide with data made available from the Western Basin Dredging and Disposal Project water quality monitoring program undertaken. Surface current speeds were greater than near-bottom currents throughout the estuary (Table 5). The maximum and mean current speeds occurred during spring periods, with maximum current speeds occurring in the deeper channels centrally located within the estuary. Reduced current speeds are experienced in the shallower intertidal regions of the estuary. Mean and maximum surface current speeds during spring tides within the mid-estuary region were 0.45 ± 0.27 m/s and 1.25 m/s, respectively, and 0.38 ± 0.21 m/s and 1.02 m/s, respectively, in the upper-estuary. Whilst near-bottom mean and maximum current speeds within the mid-estuary and upper-estuary regions were 0.35 ± 0.19 m/s and 0.77 m/s, and 0.31 ± 0.15 m/s and 0.81 m/s, respectively. In comparison, the mean and maximum surface current

speeds occurring during neap tides within the mid-estuary and upper-estuary regions were 0.35 ± 0.23 m/s and 1.13 m/s, and 0.26 ± 0.17 m/s and 0.83 m/s, respectively. Near-bottom mean and maximum current speeds in the mid-estuary and upper-estuary regions were 0.26 ± 0.14 m/s and 0.61 m/s, and 0.21 ± 0.12 m/s and 0.62 m/s, respectively.

Current directions predominantly occurred along the northwest-southeast axis, which corresponds to the orientation of the adjacent coastline (see Figure 3). The northwest and southeast currents occurred during the flood and ebb tides, respectively. In lesser instances, easterly flow components were modelled (and observed) within the estuary, for example within the mid-estuary region when ebb waters drain from South Passage Island (northwest of Station 3). Surface and near-bottom currents also demonstrated divergences in current angle. Vertical differences in current angle and speed are presumably a combined result of the wind influence on surface currents and bathymetry (deep channels amongst shallow and inter-tidal areas). Specifically, the water movement in the shallows (<5 m) would experience less steering than the movement of water in regions >5 m that is steered by the channel walls. Due to this factor there are, seemingly, instances where surface and deeper layers decouple due to the difference in momentum. Furthermore, the momentum influence is enhanced during spring tides characterised by stronger currents and greater tidal prism. The vertical variability support the selection of the three dimensional hydrodynamic model used as part of this study in capturing the depth varying current speeds and directions.

It is acknowledged that temporal extremes in flood events and prolonged periods of increased wind events (e.g., cyclonic weather systems) significantly influence current dynamics which, although irregular, should also be considered to provide a more robust approach for future predictions, especially given the importance of these events in delivering suspended material into the estuary and their influence on the regional hydrodynamics throughout Port Curtis.

5.2. Spatial and Temporal Turbidity Variations

Modelling of SSC, converted to turbidity, was undertaken to establish a predictive tool in forecasting suspended sediment concentrations (and/or turbidity levels) throughout Port Curtis estuary. The estuary typically maintains a highly turbid character [47] and during the modelling period (May–November 2010) measured turbidity levels demonstrated temporal and spatial variations, attributable to differences and interactions between factors including strength of tidal currents, water depth, bathymetry variation, proximity to the estuary entrance, grain size, and composition of benthic and suspended sediment, and fetch. Suspended sediment concentrations and turbidity levels within the estuary have been shown to demonstrate variations/trends according to wet and dry seasonal periods with greater values occurring during the wet season (*i.e.*, December to April) [77].

Mean predicted and measured surface water turbidity values within Port Curtis ranged from 4.31 ± 6.74 to 13.60 ± 12.80 NTU and 7.48 ± 15.10 to 12.62 ± 11.80 NTU, respectively. Predicted turbidity 50th and 95th percentiles ranged from 1.92 to 8.68 and 17.99 to 42.50, respectively. Surface turbidity is summarised in Table 6.

Table 5. Model-predicted surface and near-bottom current speeds based on hourly datasets. Measured dataset shown in square brackets for the mid-estuary and upper-estuary ADCP. The data is compiled from the measured and predicted datasets 07 May 2010–30 October 2010.

Estuary Region	Surface Current Speeds (m/s)								
	Spring-Neap Tides			Spring Tides			Neap Tides		
	Mean	SD	Maximum	Mean	SD	Maximum	Mean	SD	Maximum
Mid	0.40 [0.40]	0.26 [0.23]	1.25 [1.00]	0.45 [0.46]	0.27 [0.24]	1.25 [1.00]	0.35 [0.35]	0.23 [0.20]	1.13 [0.84]
Upper	0.32 [0.31]	0.19 [0.17]	1.02 [0.84]	0.38 [0.33]	0.21 [0.18]	1.02 [0.84]	0.26 [0.28]	0.17 [0.15]	0.83 [0.60]
Estuary Region	Near-Bottom Current Speed (m/s)								
	Spring-Neap Tides			Spring Tides			Neap Tides		
	Mean	SD	Maximum	Mean	SD	Maximum	Mean	SD	Maximum
Mid	0.31 [0.33]	0.17 [0.18]	0.77 [0.85]	0.35 [0.38]	0.19 [0.20]	0.77 [0.85]	0.26 [0.30]	0.14 [0.16]	0.61 [0.72]
Upper	0.26 [0.26]	0.15 [0.14]	0.81 [0.71]	0.31 [0.29]	0.15 [0.15]	0.81 [0.71]	0.21 [0.24]	0.12 [0.12]	0.62 [0.50]

Where SD represents standard deviation.

Table 6. Model-predicted turbidity summary based on hourly datasets. Measured dataset shown in square brackets. The data is compiled from the measured and predicted datasets 07 May 2010–30 October 2010.

Station	Percentile			Mean	SD	% RSD
	50th	80th	95th			
1	7.28 [5.60]	23.23 [13.30]	37.38 [25.80]	12.62 [8.51]	11.66 [10.14]	92.53 [119.25]
2	6.68 [9.00]	18.31 [19.10]	26.96 [33.90]	9.58 [12.62]	11.63 [11.80]	121.30 [93.67]
3	8.68 [9.10]	20.86 [17.40]	42.50 [31.10]	13.60 [11.58]	12.80 [9.49]	105.82 [81.90]
4	4.83 [9.05]	11.78 [17.40]	35.14 [32.00]	9.23 [11.77]	14.13 [10.75]	153.02 [91.39]
5	1.92 [10.50]	9.09 [20.10]	21.07 [34.00]	5.32 [13.35]	7.26 [10.55]	136.02 [81.42]
6	1.92 [4.40]	5.52 [9.80]	17.99 [29.60]	4.31 [7.48]	6.74 [15.10]	15.65 [20.92]

Where SD represents standard deviation and % RSD represents % relative standard deviation.

A clear spatial and temporal trend was evident as demonstrated by the datasets. Generally, turbidity was greatest in the mid- and upper-estuary stations (*i.e.*, 1–5) in comparison to the lower estuary station (6), which was positioned closest to the estuary entrance. Turbidity demonstrated high variability, particularly in the mid- and upper-estuary stations, with fluctuations in turbidity predominantly influenced by spring-neap tide variations. Turbidity was greatest throughout the estuary during spring tides due to the increased tidal energy input during this period, where peak current speeds are greatest. On a tidal cycle time-scale, greatest turbidity typically occurred during the flood tide period. To a lesser extent periods of elevated wind speeds were also shown to influence increased turbidity.

Predicted and measured turbidity levels at all sites exceeded both the Central Coast Queensland Water Quality Guideline (QWQG) regional turbidity guideline for mid-estuary and tidal canals, constructed estuaries, marinas and boat harbours (8 NTU) and upper estuarine waters (25 NTU) [78], and the Australian Water Quality Guideline (AWQG) turbidity guideline for slightly disturbed ecosystems in tropical Australia estuarine and marine waters (20 NTU) [79].

Given the good performance provided by the model in reproducing the measured turbidity levels at the six different stations and under different current and meteorological conditions within Port Curtis estuary we provide model-predicted "snapshots" of surface water turbidity (0–1 m depth) throughout the estuary. Snapshots are provided for spring and neap tide flood periods, providing example comparisons of spring and neap tide conditions (Figures 6 and 7). The snapshot images illustrate the time- and space-varying dynamics within the estuary, under sample spring and neap tide flood periods. Greatest predicted surface suspended sediment concentrations were associated within regions characterised by increased current speeds exceeding the bed shear stress, inducing suspensions and subsequent transportation of suspended sediments. Shallower intertidal regions characterised by reduced current speeds typically demonstrated decreased suspended sediment concentrations.

The results from the modelling have useful practical applications for the Port Curtis estuary, including providing predictive capabilities used in parallel with modelling of fugitive sediments from operations such as dredging and supporting selecting locations of monitoring/compliance sites. Furthermore, modelling approaches are recognised as a valuable tool for understanding and predicting sediment deposition regimes and morphological developments. Predicted zones of sediment deposition and erosion were well represented within the model during this study (model output not shown).

The model-predicted turbidity levels compared favourably with the measured surface water turbidity levels despite the exclusion of known contributing turbidity factors. The model demonstrates an ability to sufficiently predict surface water conditions (*i.e.*, suspended sediment concentrations and/or turbidity), which may be used as a standalone predictive tool, or used in a complimentary manner with event driven, source-specific modelling (e.g., dredge plume modelling). The combined model approach can be used to provide a greater understanding of future suspended sediment conditions and allow a better understanding and flexibility for compliance based operations.

The model presented clearly represents a simplified approach which does not produce all major terms in the sediment transport budget. The inclusion of such identified contributing factors present an opportunity to further refine the operational capability of the modelling approach within the Port Curtis estuary. Additionally, the inclusion of appropriate modelling routines representing light extinction presents an opportunity to broaden the scope of the model application from an ecological management standpoint by providing photosynthetic active radiation model predictions.
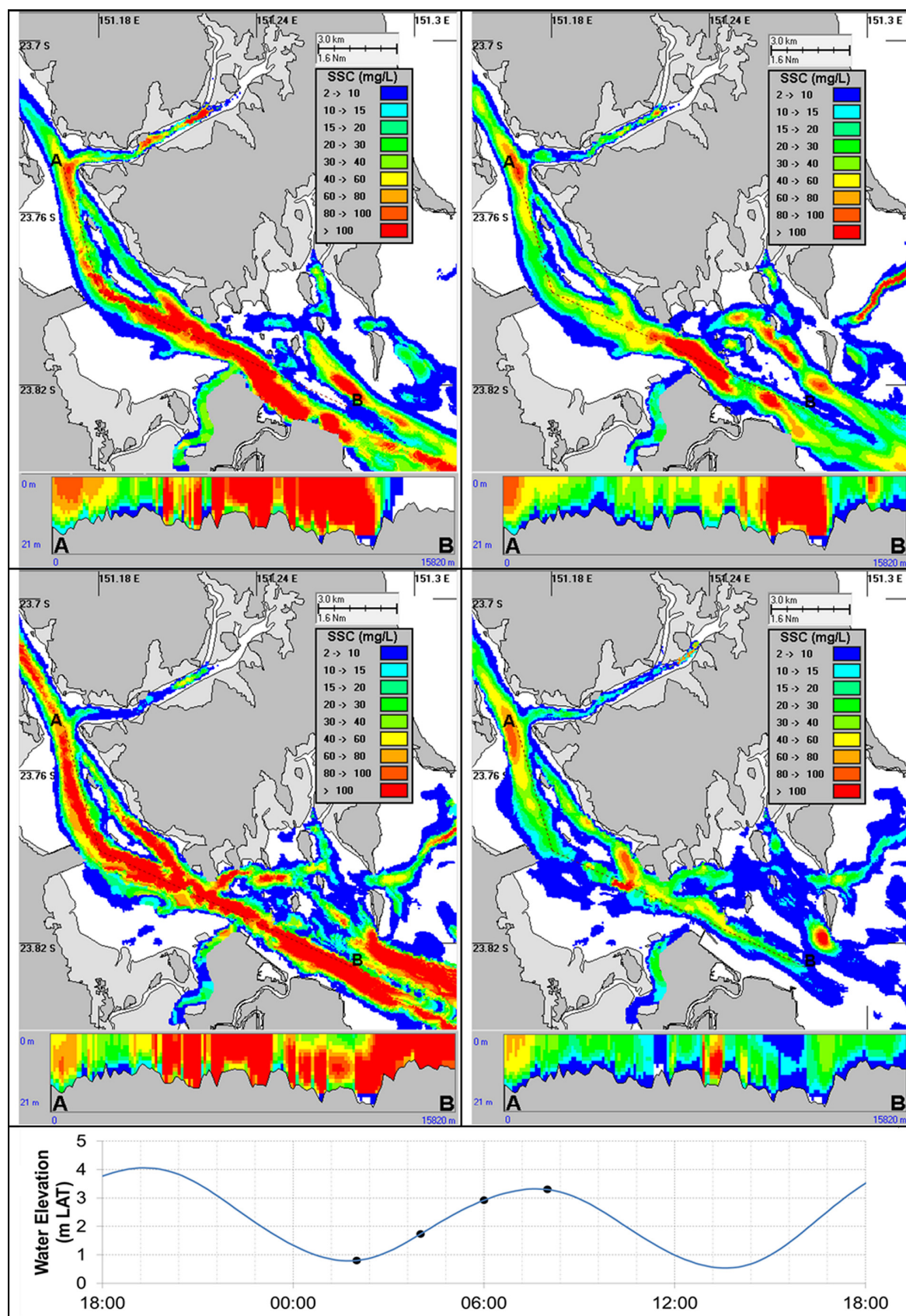
Figure 6. Model-predicted "snapshot" of surface water (0–1 m depth) suspended sediment concentrations during 02:00–08:00 from a spring tides sample flood period during 08 August 2010. The cross-section inset depicts the predicted water column suspended sediment concentrations along the transect (- - - - -) between points A and B.
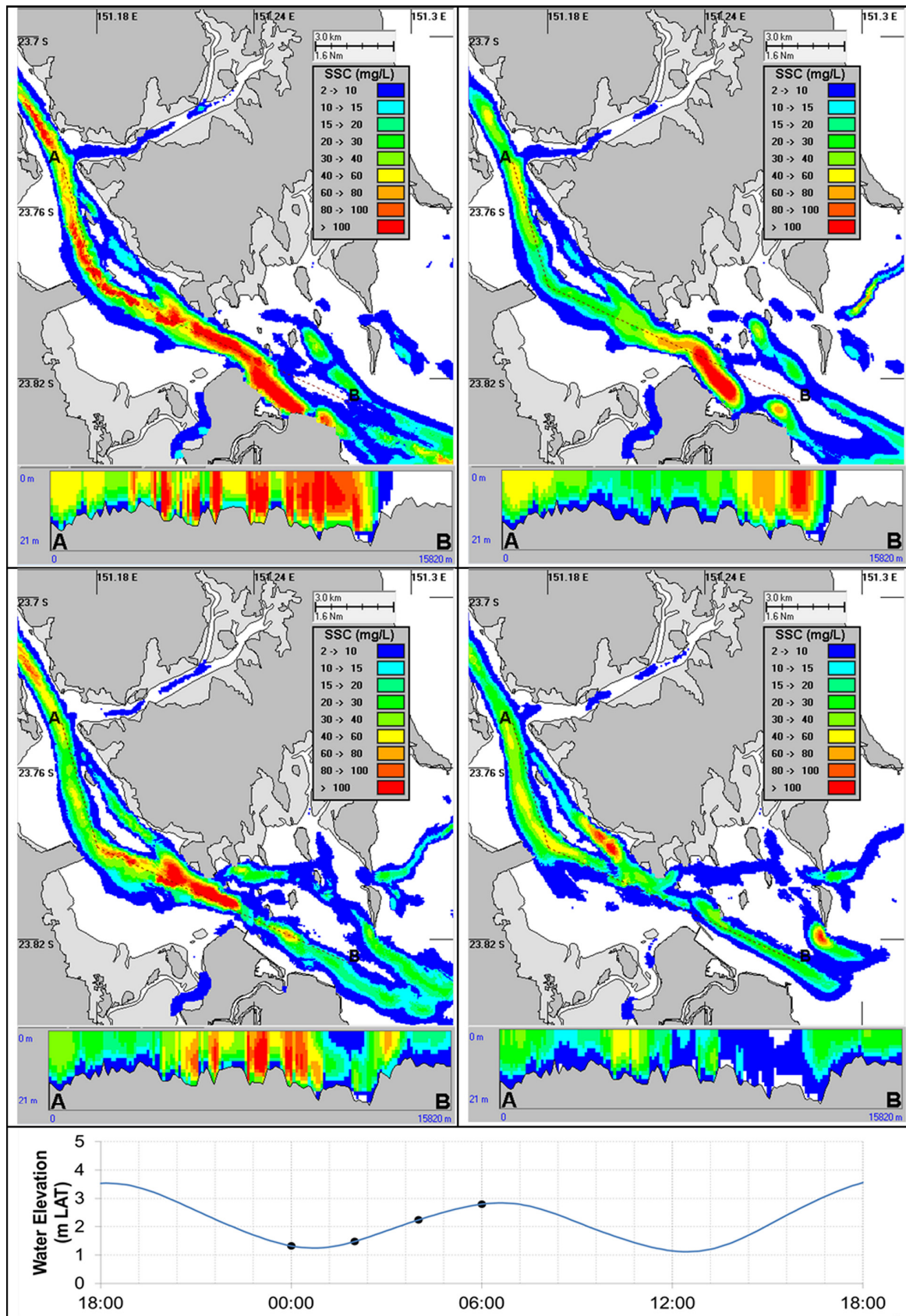
Figure 7. Model-predicted "snapshot" of surface water (0–1 m depth) suspended sediment concentrations during 00:00–06:00 from a neap tides sample flood period during 20 August 2010. The cross-section inset depicts the predicted water column suspended sediment concentrations along the transect (- - - - -) between points A and B.

6. Conclusions

A three-dimensional hydrodynamic model and wave model coupled with a sediment transport model was validated and used to investigate turbidity (suspended sediment) dynamics within a macro tidal estuary, Port Curtis. The hydrodynamic model was verified against surface and near-bottom water column measurements. In general, the simulation results accurately reproduced the variations of surface and near-bottom currents at both a mid-estuary and upper-estuary location. The three-dimensional hydrodynamic model was applied to generate forcing currents for input into the sediment transport model for the period 07 May 2010–30 October 2010. The sediment transport model predicted both the magnitudes of the turbidity levels and the modulation induced by the neap and spring tide tidal phase and wind-wave variations. The model-predicted (converted) turbidity levels compared favourably with the measured surface water turbidity levels. Predicted and measured turbidity levels at all sites exceeded both the QWQG regional turbidity guideline for mid-estuary and tidal canals, constructed estuaries, marinas and boat harbours (8 NTU) and upper estuarine waters (25 NTU), and AWQG turbidity guideline for slightly disturbed ecosystems in tropical Australia estuarine and marine waters (20 NTU). Despite the exclusion of contributing turbidity sources associated with the model, the predicted turbidity (suspended sediment) levels illustrates the importance of the tidal-induced currents and wind-wave interactions on sediment re-suspension and the applicability of the model in predicting turbidity levels within Port Curtis estuary. The inclusion of such identified contributing factors present an opportunity to further refine the operational capability of the modelling approach within the Port Curtis estuary. Following model validation the sediment transport model was used to model the spatial and temporal variability of suspended sediment concentrations within Port Curtis estuary. The results of modelling have useful practical application for the Port Curtis estuary, including providing predictive capabilities which may be used in parallel with modelling of fugitive sediments from operations such as dredging and decision support for selecting the locations for monitoring/compliance sites.

Author Contributions

R.D. and S.Z. supervised the design and planning of the model study. M.B. established the tailored sediment transport model and configured the initial surface sediment conditions source data. R.D. and S.Z. undertook the sediment transport modelling. H.-H.L. performed the scripting and statistical analyses of measured and predicted datasets. R.D. wrote the manuscript and all authors discussed the results and contributed to the manuscript.

Conflicts of Interest

The authors declare no conflict of interest.

References

1. Stumpf, R.P.; Haines, J.W. Variations in tidal level in the Gulf of Mexico and implications for tidal wetlands. *Estuar. Coast. Shelf Sci.* **1998**, *46*, 165–173.
2. Potter, I.C.; Tweedley, J.R.; Elliott, M.; Whitfield, A.K. The ways in which fish use estuaries: A refinement and expansion of the guild approach. *Fish Fish.* **2013**, *16*, 230–239.
3. Sheaves, M.; Baker, R.; Nagelkerken, I.; Connolly, R.M. True value of estuarine and coastal nurseries for fish: Incorporating complexity and dynamics. *Estuar. Coasts* **2014**, *38*, 401–414.
4. De la Paz, M.; Gómez-Parra, A.; Forja, J. Tidal-to-seasonal variability in the parameters of the carbonate system in a shallow tidal creek influenced by anthropogenic inputs, Rio San Pedro (SW Iberian Peninsula). *Cont. Shelf Res.* **2008**, *28*, 1394–1404.
5. Roy, P.S.; Williams, R.J.; Jones, A.R.; Yassini, I.; Gibbs, P.J.; Coates, B.; West, R.J.; Scanes, P.R.; Hudson, J.P.; Nichol, S. Structure and function of south-east Australian estuaries. *Estuar. Coast. Shelf Sci.* **2001**, *53*, 351–384.
6. Barbier, E.B.; Hacker, S.D.; Kennedy, C.; Koch, E.W.; Stier, A.C.; Silliman, B.R. The value of estuarine and coastal ecosystem services. *Ecol. Monogr.* **2011**, *81*, 169–193.
7. Zhang, K.; Liu, H.; Li, Y.; Xu, H.; Shen, J.; Rhome, J.; Smith III, T.J. The role of mangroves in attenuating storm surges. *Estuar. Coast. Shelf Sci.* **2012**, *102*, 11–23.
8. Gedan, K.B.; Kirwan, M.L.; Wolanski, E.; Barbier, B.B.; Silliman, B.R. The present and future role of coastal wetland vegetation in protecting shorelines: Answering recent challenges to the paradigm. *Clim. Chang.* **2011**, *106*, 7–29.
9. Wang, X.H.; Pinardi, N. Modeling the dynamics of sediment transport and resuspension in the northern Adriatic Sea. *J. Geophys. Res.* **2002**, *107*, doi:10.1029/2001JC001303.
10. Vandermeulen, J.H. Environmental trends in ports and harbours: Implications for planning and management. *Maritime Policy Manag.* **1996**, *23*, 55–66.
11. Machiwa, J.F. Anthropogenic pollution in the Dar es Salaam harbour area, Tanzania. *Mar. Pollut. Bull.* **1992**, *24*, 562–567.
12. Oviatt, C.A.; Nixon, S.W. Sediment resuspension and deposition in Narrangansett Bay. *Estuar. Coast. Mar. Sci.* **1975**, *3*, 201–217.
13. Black, K.S. Suspended sediment dynamics and bed erosion in the high shore mudflat region of the Humber Estuary, UK. *Mar. Pollut. Bull.* **1998**, *37*, 122–133.
14. Allan, J.R.L.; Duffy, M.J. Medium-term sedimentation on high intertidal mudflats and salt marshes in the Severn Estuary, SW Britain: The role of wind and tide. *Mar. Geol.* **1998**, *150*, 1–27.
15. Regnier, P.; Wollast, R. Distribution of trace metals in suspended matter of the Scheldt estuary. *Mar. Chem.* **1993**, *43*, 3–19.
16. Christiansen, C.; Gertz, F.; Laima, M.J.C.; Lund-Hansen, L.C.; Vang, T.; Jürgensen, C. Nutrient (P, N) dynamics in the southwestern Kattegat, Scandinavia: Sedimentation and resuspension effects. *Environ. Geol.* **1997**, *29*, 66–77.

17. Cloern, J.E.; Nichols, F.H. Time scales and mechanisms of estuarine variability, a synthesis from studies of San Francisco Bay. *Hyrdobiologia* **1985**, *129*, 229–237.

18. Morin, J.; Morse, J.W. Ammonium release from resuspended sediments in the Laguna Madre estuary. *Mar. Chem.* **1999**, *65*, 97–110.

19. Tengberg, A.; Almroth, E.; Hall, P. Resuspension and its effects on organic carbon recycling and nutrient exchange in coastal sediments: *In situ* measurements using new experimental technology. *J. Exp. Mar. Biol. Ecol.* **2003**, *285*, 119–142.

20. Anthony, K.R.N.; Ridd, P.V.; Orpin, A.R.; Larcombe, P.; Lough, J. Temporal variation of light availability in coastal benthic habitats: Effects of clouds, turbidity, and tides. *Limnol. Oceanogr.* **2004**, *49*, 2201–2211.

21. Devlin, M.J.; Barry, J.; Mills, D.K.; Gowen, R.J.; Foden, J.; Sivyer, D.; Tett, P. Relationships between suspended particulate material, light attenuation and Secchi depth in UK marine waters. *Estuar. Coast. Shelf Sci.* **2008**, *79*, 429–439.

22. Liu, W.-C.; Hsu, M.-H.; Kuo, A.Y. Modelling of hydrodynamics and cohesive sediment transport in Tanshui River estuarine system, Taiwan. *Mar. Pollut. Bull.* **2002**, *44*, 1076–1088.

23. Wilbur, D.H.; Clarke, D.G. Biological effects of suspended sediments: A review of suspended sediment impacts on fish and shellfish with relation to dredging activities in estuaries. *North Am. J. Fish. Manag.* **2001**, *21*, 855–875.

24. Wong, C.K.; Pak, I.A.P.; Liu, X.J. Gill damage to juvenile orange-spotted grouper *Epinephelus coioides* (Hamilton, 1822) following exposure to suspended sediments. *Aquac. Res.* **2013**, *44*, 1865–1695.

25. Norkko, J.; Hewitt, J.E.; Thrush, S.F. Effects of increased sedimentation on the physiology of two estuarine soft-sediment bivalves, *Austrovenus stutchburyi* and *Paphies australis*. *J. Exp. Mar. Biol. Ecol.* **2006**, *333*, 12–26.

26. Droppo, I.G.; Krishnappan, B.G.; Liss, S.N.; Marvin, C.; Biberhofer, J. Modelling sediment-microbial dynamics in the South Nation River, Ontario, Canada: Towards the prediction of aquatic and human health risk. *Water Res.* **2011**, *45*, 3797–3809.

27. Lopes, J.F.; Dias, J.M.; Dekeyser, I. Numerical modeling of cohesive sediments transport in the Ria de Aveirolagoon, Portugal. *J. Hydrol.* **2006**, *319*, 176–198.

28. Andutta, F.P.; Wang, X.H.; Li, L.; Williams, D. Hydrodynamics and sediment transport in a macro-tidal estuary: Darwin Harbour, Australia. In *Estuaries of Australia in 2050 and Beyond*; Wolanski, E., Ed.; Springer: Dordrecht, The Netherlands, 2014; pp. 111–129.

29. Ali, A.; Lemckert, C.J.; Zhang, H.; Dunn, R.J.K. Sediment Dynamics of a Very Shallow Subtropical Estuarine Lake. *J. Coast. Res.* **2010**, *26*, 436–443.

30. Brand, A.; Lacy, J.R.; Hsu, K.; Hoover, D.; Gladding, S.; Stacey, M.T. Wind-enhanced resuspension in the shallow waters of South San Francisco Bay: Mechanisms and potential implications for cohesive sediment transport. *J. Geophys. Res.* **2010**, *115*, C11024.

31. Giardino, A.; Ibrahim, E.; Adam, S.; Toorman, E.A.; Monbaliu, J. Hydrodynamics and cohesive sediment transport in the Ijzer estuary, Belgium: Case study. *J. Waterw. Port Coast. Ocean Eng.* **2009**, *135*, 176–184.

32. Guan, W.B.; Wolanski, E.; Dong, L.X. Cohesive sediment transport in the Jiaojiang River estuary, China. *Estuar. Coast. Shelf Sci.* **1998**, *46*, 861–871.

33. Hayter, E.J.; Mehta, A.J. Modelling cohesive sediment transport in estuarial waters. *Appl. Math. Model.* **1986**, *10*, 294–303.

34. Carniello, L.; Defina, A.; D'Alpaos, L. Modeling sand-mud transport induced by tidal currents and wind waves in shallow microtidal basins: Application to the Venice Lagoon (Italy). *Estuar. Coast. Shelf Sci.* **2012**, *102*, 105–115.

35. Cancino, L.; Neves, R. Hydrodynamic and sediment suspension modelling in estuarine systems: Part II. Application to the Western Scheldt and Gironde estuaries. *J. Mar. Syst.* **1999**, *22*, 117–131.

36. Lumborg, U. Cohesive sediment transport modelling application to the Lister Dyb tidal area in the Danish Wadden Sea. *J. Coast. Res.* **2004**, *SI 41*, 114–123.

37. Le Normant, C. Three-dimensional modelling of cohesive sediment transport in the Loire estuary. *Hydrol. Process.* **2000**, *14*, 2231–2243.

38. Lumborg, U.; Pejrup, M. Modelling of cohesive sediment transport in a tidal lagoon—An annual budget. *Mar. Geol.* **2005**, *218*, 1–16.

39. Gladstone Ports Corporation Ltd. History of the Gladstone Ports Corporation limited. Available online: http://www.gpcl.com.au/AboutGPC/HistoryofGPC.aspx (accessed on 23 March 2015).

40. Walker, M.H. *Fisheries Resources of the Port Curtis and Capricorn Regions*; Queensland Fisheries Management Authority: Brisbane, Australia, 1997.

41. Connolly, R.M.; Currie, D.R.; Danaher, K.F.; Dunning, M.; Melzer, A.; Platten, J.R.; Shearer, D.; Stratford, P.J.; Teasdale, P.R.; Vadergradt, M. *Intertidal Wetlands of Port Curtis: Ecological Patterns and Processes and Their Implications*; Research Centre for Coastal Zone, Estuary and Waterway Management: Brisbane, Australia, 2006.

42. Connolly, R.M.; Guest, M.A. *Critical Estuarine Habitats for Food Webs Supporting Fisheries in Port Curtis, Central Queensland, Australia*; Griffith University and the Cooperative Research Centre for Coastal Zone, Estuary and Waterway Management: Brisbane, Australia, 2004.

43. Jones, M-A.; stauber, J.; Apte, S.; Simpson, S.; Vicente-Beckett, V.; Johnson, R.; Duivenvoorden, L. A risk assessment approach to contaminants in Port Curtis, Queensland, Australia. *Mar. Pollut. Bull.* **2005**, *51*, 448–458.

44. Anastasi, A.; Wilson, S.P. A review of manganese in subtropical estuaries: Port Curtis—A case study. *Australas. J. Ecotoxicol.* **2010**, *16*, 119–133.

45. Andersen, L.; Norton, J. *Port Curtis Mud Crab shell Disease: Nature, Distribution and Management*; Central Queensland University: Gladstone, Australia, 2001.

46. Angel, B.; Hales, L.T.; Simpson, S.L.; Apte, S.S.; Chariton, A.A.; Shearer, D.; Jolley, D.F. Spatial variability of cadmium, copper, manganese, nickel and zinc in the Port Curtis Estuary, Queensland, Australia. *Mar. Freshw. Res.* **2010**, *61*,170–183.

47. Herzfeld, M.; Parslow, J.; Andrewartha, J.; Sakov, P.; Webster, I.T. *Hydrodynamic Modelling of the Port Curtis Region*; Research Centre for Coastal Zone, Estuary and Waterway Management: Brisbane, Australia, 2004.

48. Johnson, B.H.; Andersen, E.; Isaji, T.; Teeter, A.M.; Clarke, D.G. *Description of the SSFATE Numerical Modeling System*; U.S. Army Engineer Research and Development Centre: Vicksburg, MS, USA, 2000.

49. Deltares. *Delft3D-FLOW User Manual, Version 3.15.34158*; Deltares: Rotterdamseweg, The Netherlands, 2014; pp. 1–684.

50. Pan, L.; Ding, P.; Ge, J. Impacts of deep waterway project on morphological changes within the north passage of the Changjiang estuary, China. *J. Coast. Res*. **2012**, *28*, 1165–1176.

51. Chen, Q.; Mynett, A.E. Modelling algal blooms in the Dutch coastal waters by integrated numerical and fuzzy cellular automata approaches. *Ecol. Model.* **2006**, *199*, 73–81.

52. Asia-Pacific ASA Pty Ltd. Asia-Pacific ASA Pty Ltd, Gold Coast, Australia. Unpublished work, 2010.

53. Wolanski, E.; Jones, M.; Bunt, J.S. Hydrodynamics of a tidal creek-mangrove swamp system. *Aust. J. Mar. Freshwater Res.* **1980**, *31*, 431–450.

54. King, B.; Wolanski, E. Bottom friction reduction in turbid estuaries. In *Coastal and Estuarine Studies*; Prandle, D., Ed.; American Geophysical Union: Washington, DC, 1996; Volume 50, pp. 325–337.

55. Booij, N.; Ris, R.C.; Holthuijsen, L.H. A third-generation wave model for coastal regions: 1. Model description and validation. *J. Geophys. Res. Oceans* **1999**, *104*, 7649–7666.

56. Tolman, H.L. *User Manual and System Documentation of WAVEWATCH-III, Version 2.22*; U.S. Department of Commerce, NOAA, Environmental Modelling Centre Marine Modelling and Analysis Branch: Washington, DC, USA, 2002; pp. 1–133.

57. Eldeberky, Y.; Battjes, J.A. Spectral modelling of wave breaking: Application to Boussinesq equations. *J. Geophys. Res.* **1996**, *101*, 1253–1264.

58. Collins, J.I. Prediction of shallow water spectra. *J. Geophys. Res.* **1972**, *77*, 2693–2707.

59. Howlett, E. GIS-based tools in support of Dredging Operations. *Sea Technol.* **2003**, *44*, 42–44

60. Spearman, J.; Bray, R.N.; Burt, J.L.; Burt, T.N.; Mead, C.T.; Scott, D. Plume dispersion modelling using dynamic representation of trailer dredger source terms. *Proc. Mar. Sci.* **2007**, *8*, 417–448.

61. Swanson, J.C.; Isaji, T.; Galagan, C. Modeling the Ultimate Transport and Fate of Dredge-Induced Suspended Sediment Transport and Deposition. In Proceedings of the WODCON XVIII 27, Lake Buena Vista, FL, USA, 27 May–1 June 2007.

62. Soulsby, R.L. *Dynamics of Marine Sands: A Manual for Practical Application*; Thomas Telford: London, UK, 1997; pp. 1–249.

63. Sanford, L.P.; Maa, J.P.-Y. A unified erosion formulation for fine sediments. *Mar. Geol.* **2001**, *179*, 9–23.

64. Lin, J.; Wang, H.V.; Oh, J.-H.; Park, K.; Kim, S.-C.; Shen, J.; Kuo, A.Y. A new approach to model sediment resuspension in tidal estuaries. *J. Coast. Res.* **2003**, *19*, 76–88.

65. Van Rijn, L.C. *Handbook Sediment Transport by Currents and Waves*, 2nd ed.; Delft Hydraulic. Lab: Delft, The Netherlands, 1989; pp. 1–307.

66. GeoCoastal Australia Pty Ltd. GeoCoastal Australia Pty Ltd, Brisbane, Australia. Unpublished work, 2010.

67. Bartier P.M.; Keller, P.C.; Multivariate interpolation to incorporate thematic surface data using inverse distance weighting (IDW). *Comput. Geosci.* **1996**, *22*, 795–799.

68. Ward, L.G.; Kemp, W.M.; Boynton, W.R. The influence of waves and seagrass communities on suspended particulates in an estuarine embayment. *Maine Geol.* **1984**, *59*, 85–103.

69. Wood, R.; Widdows, J. A model of sediment transport over an intertidal transect, comparing the influences of biological and physical factors. *Limnol. Oceanogr.* **2002**, *47*, 848–855.

70. Nowell, A.R.M.; Jumars, P.A.; Eckman, J.E. Effects of biological activity on the entrainment of marine sediments. *Marine Geol.* **1981**, *42*, 133–153.

71. Environmetrics Australia Pty Ltd. Environmetrics Australia Pty Ltd, Beaumaris, Australia. Unpublished work, 2010.

72. Willmott, C.J. On the Validation of Models. *Phys. Geogr.* **1981**, *2*, 184–194.

73. Willmott, C.J.; Matsuura, K. Advantages of the mean absolute error (MAE) over the root mean square error (RMSE) in assessing average model performance. *Clim. Res.* **2005**, *30*, 79–82.

74. Gladstone Wave Monitoring. Available online: http://www.qld.gov.au/environment/coasts-waterways/beach/waves-sites/gladstone/ (accessed on 3 March 2015).

75. Climate Statistics for Australian Locations: Summary statistics Gladstone airport. Available online: http://www.bom.gov.au/climate/averages/tables/cw_039326.shtml (accessed on 5 March 2015).

76. GHD Pty Ltd. *Western Basin Dredging and Disposal Project Chapter 6—Hydrodynamic Modelling*; GHD Pty Ltd/Gladstone Ports Corporation: Brisbane, Australia, 2010.

77. Vision Environment (QLD) Pty Ltd. *Western Basin Dredging and Disposal Project Water quality Monitoring*; Vision Environment: Gladstone, Australia, 2012; pp. 1–89.

78. Department of Environment and Heritage Protection. *Queensland Water Quality Guidelines, Version 3*; Department of Environment and Heritage Protection: Brisbane, Australia, 2009; pp. 1–184.

79. Australia and New Zealand Environment and Conservation Council (ANZECC)/Agriculture and Resource Management Council of Australia and New Zealand (ARMCANZ). *Australian and New Zealand Guidelines for Fresh and Marine Water Quality Volume 2—Rationale and Background Information*; ANZECC/ARMCANZ: Canberra, Australia, 2000.